Supporting Information

Wang et al. 10.1073/pnas.1601465113

SI Text

Further Details of the Mijiaya Site. The Mijiaya site was discovered in 1923 by J. G. Anderson and excavated from 2004 to 2006. The excavations revealed three separate cultural strata belonging to established chronology in the region based on ceramic typology with associated radiocarbon dates: the Banpo IV phase (belonging to the late Yangshao period, 3400–2900 BC), the Miaodigou II phase (2800–2450 B.C) (36), and the Keshengzhuang phase (2400–2000 BC) (37). The entire site measures around 45 ha with cultural deposits 1.5–4 m in depth. A total of 166 Banpo IV pits were found, and the majority of them are regular in shape with flat bottoms, suggesting their initial function as storage pits (8). The ceramic artifacts from the earliest stratum are Banpo IV styles that are comparable to the related sites in the region, including Xiehu in Lantian, Xijing in Shanxian, and Quanhucun in Huaxian. Pollen analysis indicates that the climate of the Wei River valley was semiarid during the Banpo IV phase, characterized by steppe vegetation and herbaceous plants dominating the pollen assemblage (38).

Social Complexity During the Late Yangshao Period. The settlement pattern of the late Yangshao period is characterized by site nucleation and a two- or three-tiered settlement hierarchy. Several large regional centers emerged along the Wei River valley for the first time, including Dadiwan (100 ha) and Gaositou in Gansu and Anban (70 ha) in Shaanxi. Palace-like architectures are present in all three sites, occupying the central locations of the settlements. At Dadiwan, for example, a multiroomed structure (F901; 290 m^2 in size) was found in the center of the site (39). Ceramic remains found in the structure include large-sized pottery storage urns, pile-up bowls, and vessels of regularly graduated sizes. A large hearth was located in the center of the major room. The house may have functioned as a central place for activities of regional communities. Compared with the sites in the middle Yangshao period, public buildings in the late Yangshao period became bigger in size, and they are likely to have served for ritual ceremonies and feasting, at both local and regional levels (34). The construction of large public buildings during the late Yangshao period implies an increased level of social hierarchy and complexity. Competitive feasting is likely to have been conducted by the regional elite for obtaining high social status.

SI Materials and Methods

Field Sampling. The field sampling took place in the Jingwei Archaeological Station in Xi'an, China. All artifacts for this study were curated in storage. Only new and sterile plastic bags, test tubes, pipettes, toothbrushes, and razor blades were used during the sampling process. The procedure used is as follows.

First, three residue samples for IC analysis were taken from the interior surfaces of Funnel 1, Pot 3, and Pot 5. The residues were yellowish in color and firmly adhering to the interior vessel walls. Residues from each vessel were scrapped off by using a clean razor blade. By using the same method, two control samples were obtained from the soil adhering to the exterior surface of Pot 5 (one for IC and one for microbotanical analysis), and one control sample was taken from the conservation plaster material on the interior surface of Funnel 2.

Second, all artifacts were subjected to sonication. An ultrasound bath was used to extract residues from Funnel 1, Funnel 2, Pot 1, and a control sample (stone adze). Each artifact was placed in a new, polyvinyl bag with ~15 mL of distilled water. For Funnel 1, Funnel 2, and Pot 1, only the mouth part (up to 2.5–3 cm from the opening) was immersed in the distilled water. For the stone adze, the entire artifact was immersed. The bag containing the artifact then was placed into the bath for 3 min. After 3 min, the artifact was removed from the bag. For artifacts that were too big to be placed in the ultrasound bath (Pot 2, Pot 3, Pot 4, Pot 5, Pot 6, Pot7), ultrasonic toothbrushes were used. First, each artifact was placed in a new polyvinyl bag. The interior surface of the artifact was then brushed gently with an ultrasonic toothbrush and at the same time a pipette was used to add distilled water to rinse the surface. Only a new ultrasonic toothbrush and a new pipette were used for each artifact. The water and all sediment from the bag were transferred into a new 15-mL test tube. Each tube was stored in a sealed plastic bag before laboratory analysis.

Laboratory Techniques for Starch and Phytolith Analyses. The protocol for starch and phytolith extraction is as follows:

Sample concentration. Each 15-mL tube containing sediment and water was topped off with distilled water and placed in a centrifuge (Eppendorf 5804, Hamburg, Germany) for 5 min at 1,500 rpm to concentrate the sample at the bottom of the tube. The supernatant was then decanted.

Dispersion. Four microliters of 0.1% EDTA ($Na_2EDTA{\bullet}2H_2O$) solution was added to each tube. Then the capped tubes were placed in an automatic shaker for 2 h to disperse the sediments. After being removed from the shaker, the tubes were filled to 15 mL with distilled water and centrifuged for 5 min at 1,500 rpm, and the supernatant was decanted.

Heavy liquid separation. Four microliters of heavy liquid sodium polytungstate at a specific gravity of 2.35 was added to the tubes. The tubes were then centrifuged for 15 min at 1,000 rpm. The top 1- to 2-mm layer of organics was carefully removed from each test tube by a new pipette and then transferred into a new 15-mL tube. The samples were topped off with distilled water and centrifuged for 5 min at 1,500 rpm to concentrate the starch and phytolith at the bottom of the tube, and the supernatant was decanted. The rinse was repeated two more times to remove any remaining sodium polytungstate.

Slide mounts and microscope scanning. An aliquot of residue sample was extracted with a pipette to a microscope slide and allowed to dry. Then the residue was resuspended in 30–40 μL of 50% (vol/vol) glycerol and 50% (vol/vol) distilled water. A coverslip was placed on top, and the edges were sealed with nail polish. All slides were scanned under a Zeiss Axio Scope A1 fitted with polarizing filters and DIC optics, at 200× and 400× for both starch and phytoliths.

Beer-Brewing Experiments. The brewing experiments were based on four sets of cereal grains. The four experimental sets consisted of broomcorn millet (40 g), foxtail millet (40 g), a mixture of broomcorn millet (30 g) and barley (10 g), and a mixture of foxtail millet (30 g) and barley (10 g), respectively. Each set went through three brewing steps, including malting, mashing and fermentation. The procedure is as follows:

First, grains were immersed in water until they began to germinate. The room temperature was around 20–28 °C. Most grains germinated after 8 d, and they were drained and dried. Next, the malted grains were crushed and mixed with heated water to achieve a final temperature of 65 °C. The temperature was maintained for 2 h. Finally, the mash was cooled in room temperature and allowed to ferment in a brewing container for 2 d. During fermentation each container was covered with a lid to create an anaerobic condition.

To obtain reference starch samples to compare with the ancient starches, we took starch samples during the experiment. Two to three malted seeds of broomcorn millet, foxtail millet, and barley were taken for microscopic observation, and two patterns were observed. First, all three types of malted grains had starches that

showed pittings, channelings, or fissures radiating from their centers. The centers of the grains appeared hollowed but the outer edges appeared undamaged (Fig. S3 *A*–*C*). Second, this type of damage was common and appeared in around 90% of broomcorn millet and foxtail millet starches; it was rare and appeared in about 1% of barley starches. A second batch of starch samples was taken from each set when mashing was done. Various levels of swelling and distortion were present in ∼5% of broomcorn millet, and 10–15% of the other three samples (Fig. S3 *D*, *G*, *J*, and *M*). When fermentation was finished, a third batch of starch samples was taken from each set. Three patterns were observed from all four brewing sets. First, pitted starch grains were still present, and their outer edges also appeared damaged (see arrows in Fig. S3 *E*, *H*, and *K*). Second, abundant starch grains exhibited swelling, distortion, and loss of extinction cross. Many starch grains merged into one another completely (Fig. S3 *F* and *O*). Compared with mashed samples, the fermented starch grains exhibited a higher level of swelling and distortion; extinction cross was not observed in many large starches. Third, some small-sized starch grains remained intact (see arrow in Fig. S3*L*). However, we were unable to produce quantified data from the fermented samples because a high proportion of the starch grains was gelatinized and merged together.

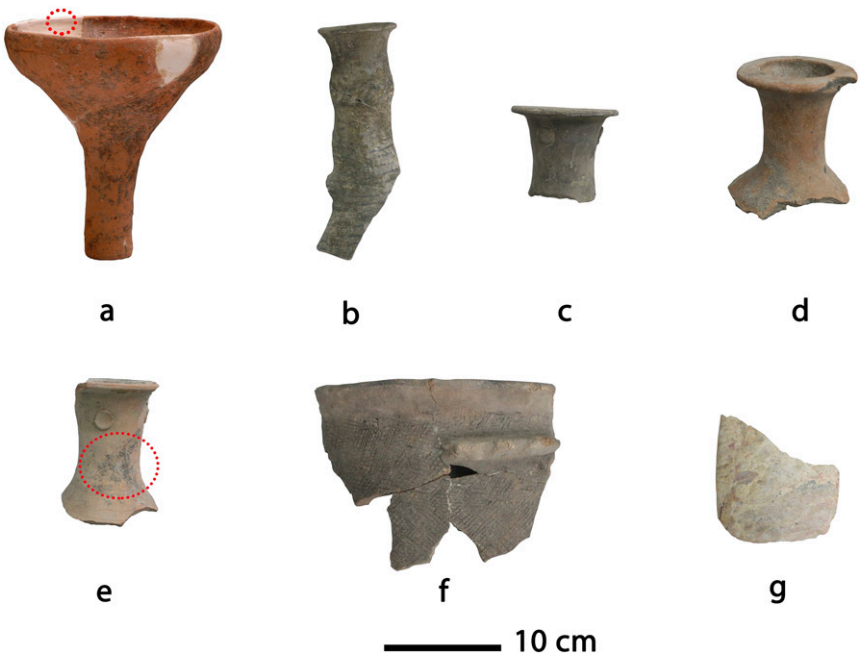

Fig. S1. Analyzed Mijiaya artifacts not included in Fig. 1. Artifacts and their discovery contexts from the upper row to the lower row: (*A*) funnel 2 (H78), red circle indicating the sampling location of control sample 3; (*B*) pot 1 (H82); (*C*) pot 2 (H82); (*D*) pot 4 (H82); (*E*) pot 5 (H78), red circle indicating the sampling location of control sample 1 and control sample 4; (*F*) pot 7 (H78); (*G*) stone adze (H78).

Fig. S2. Residues from the interior surface of funnel 1.

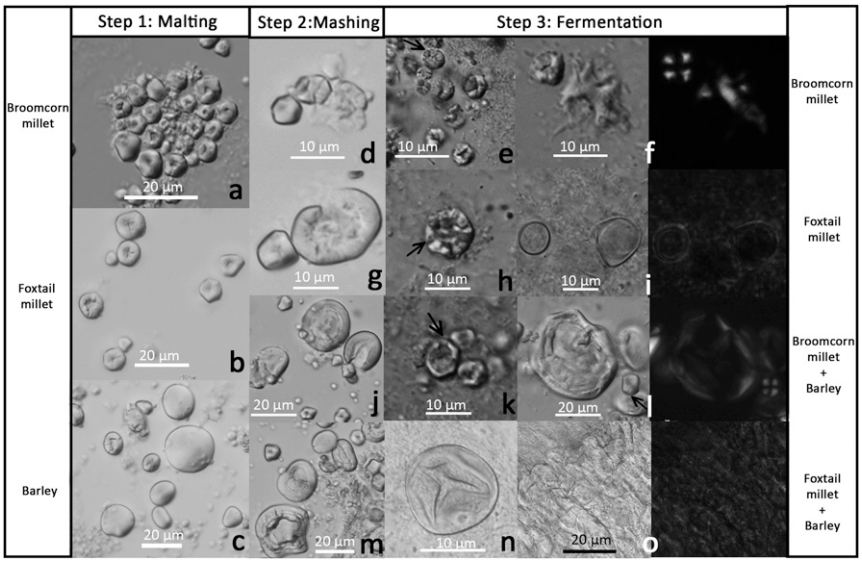

Fig. S3. Starch grains from brewing experiments: (*A*) Malted broomcorn millet (*P. miliaceum*); (*B*) malted foxtail millet (*S. italica*); (*C*) malted barley (*H. vulgare*); (*D*) mashed broomcorn millet; (*E*) fermented broomcorn millet, showing pittings and damaged outer edges; (*F*) fermented broomcorn millet, showing pitting (*Left*) and gelatinization (*Right*); (*G*) mashed foxtail millet; (*H*) fermented foxtail millet, showing pitting and damaged outer edge; (*I*) fermented foxtail millet, showing gelatinization, merging, and loss of extinction cross; (*J*) mashed broomcorn millet and barley; (*K*) fermented broomcorn millet and barley, showing big hollows in the centers and damaged outer edges; (*L*) fermented broomcorn millet and barley, showing one gelatinized grain (*Left*) and one undamaged grain (*Right*); (*M*) mashed foxtail millet and barley; (*N*) a starch grain from fermented foxtail millet and barley, showing channeling and distortion; (*O*) a cluster of completely merged starch grains and loss of extinction cross from fermented foxtail millet and barley.

Table S1. Morphology of starch grains

ID	Grain shape	Size range (mean), μm	Hilum	Fissures	Lamellae	Extinction cross
Broomcorn millet, *P. miliaceum*	Polygonal and subround, facetted	3.77–13.87 (9.06)	Mostly centric	"Y", "V", or linear forms	Absent	"+" Shape with straight arms
Triticeae	Round or oval, flat surface	6.85–38.38(21.30)	Centric	Rare	Visible on large grains	Mostly "+" shape
Job's tears, *C. lacryma-jobi*	Polygonal and subround, facetted	5.1–28.28(16.3)	Centric or eccentric	Common, "Y", "V", and linear forms, or many fine lines radiating to the edge	Visible on some	Mostly straight, sometimes with bent or Z-shaped arms
Snake gourd root, *T. kirilowii*	Spherical or regular oval, bell-shape, semispherical, and nearly semispherical with facets	8.61–30.61(18.85)	Centric or eccentric	Some with short linear fissure	Visible on large grains	Mostly with bent arms, sometimes straight
Yam, *Dioscorea* sp.	Irregular triangular or oval shape	12.34–23.11(18.09)	Eccentric	Some with short linear fissure	Visible on most grains	Bent arms
Lily, *Lilium* sp.	Irregular triangular	16.88–34.71(24.41)	Eccentric	Some with short linear fissure	Visible on most grains	Bent arms

Table S2. Description of phytolith morphometries analyzed

Name	Description
Form factor	Equals 4 × Area × π/Perimeter, it is 1.0 for a perfect circle and diminishes for irregular shapes.
Roundness	Equals 4 × Area/π × Length^2, it is 1.0 for perfect circle and diminishes with elongation of the feature.
Solidity	Ratio of area to convex area; It is 1.0 for a perfectly convex shape, diminishes if there are surface indentations.
Compactness	Ratio of the equivalent diameter to the length.
Convexity	Ratio of convex perimeter to perimeter; It is 1.0 for a perfectly convex shape, diminishes if there are surface indentations.
Aspect ratio	Equals length/width.

Table S3. Range of mean morphometries of articulated dendritic wave lobes observed in all bract types from all inflorescence locations for all accessions of selected species from modern comparative species: *Triticum*, *Avena*, *Secale*, *Agropyron*, and *Bromus*

Genus	*Triticum*					*Avena*	*Secale*	*Agropyron*		*Bromus*
Species	*T. aestivum*	*T. dicoccoides*	*T. dicoccon*	*T. durum*	*T. monococcum*	*A. sativa*	*S. cereale*	*A. cristatum*	*A. mongolicum*	*B. japonica*
Form factor	0.607–0.725	0.646–0.711	0.643–0.745	0.623–0.707	0.668–0.817	0.635–0.721	0.635–0.709	0.691–0.744	0.672–0.711	0.680–0.739
Roundness	0.500–0.614	0.517–0.608	0.531–0.619	0.552–0.603	0.532–0.617	0.526–0.616	0.504–0.626	0.526–0.603	0.512–0.594	0.537–0.614
Solidity	0.936–0.973	0.940–0.970	0.918–0.979	0.922–0.957	0.954–0.984	0.904–0.978	0.928–0.968	0.966–0.979	0.952–0.972	0.963–0.974
Compactness	0.691–0.781	0.714–0.777	0.724–0.785	0.738–0.769	0.725–0.783	0.718–0.783	0.706–0.774	0.738–0.774	0.712–0.769	0.730–0.782
Convexity	0.921–0.944	0.912–0.941	0.905–0.948	0.889–0.940	0.935–0.949	0.907–0.946	0.922–0.942	0.937–0.948	0.937–0.944	0.941–0.947
Aspect ratio	1.463–1.638	1.469–1.710	1.500–1.667	1.463–1.611	1.490–1.710	1.423–1.775	1.503–1.690	1.482–1.826	1.458–1.758	1.435–1.641

Table S4. Range of mean morphometries of articulated dendritic wave lobes observed in all bract types from all inflorescence locations for all accessions of selected species from modern comparative species: *Elytrigia*, *Leymus*, *Roegneria*, *Hordeum*

Genus	*Elytrigia*	*Leymus*	*Roegneria*			*Hordeum*				
Species	*E. elongata*	*L. secalinus*	*R. mayebarana*	*R. ciliaris*	*R. pendulina*	*H. vulgare*	*H. bulbosum*	*H. comosum*	*H. secalinum*	*H. distichon*
Form factor	0.719–0.742	0.706–0.740	0.705–0.741	0.719–0.737	0.621–0.746	0.644–0.736	0.708–0.757	0.717–0.744	0.693–0.760	0.642–0.748
Roundness	0.582–0.628	0.573–0.625	0.552–0.603	0.588–0.613	0.621–0.629	0.448–0.617	0.563–0.632	0.564–0.634	0.525–0.644	0.458–0.626
Solidity	0.965–0.983	0.960–0.973	0.967–0.978	0.972–0.980	0.969–0.976	0.954–0.981	0.977–0.988	0.971–0.977	0.978–0.983	0.979–0.985
Compactness	0.760–0.791	0.754–0.789	0.741–0.774	0.765–0.782	0.786–0.792	0.664–0.784	0.748–0.794	0.748–0.796	0.721–0.802	0.671–0.790
Convexity	0.941–0.948	0.939–0.946	0.943–0.949	0.942–0.947	0.945–0.946	0.934–0.952	0.943–0.950	0.943–0.945	0.945–0.950	0.945–0.948
Aspect ratio	1.412–1.580	1.392–1.562	1.489–1.641	1.463–1.544	1.414–1.449	1.497–2.090	1.458–1.657	1.449–1.707	1.410–1.829	1.482–2.123

Table S5. Mean morphometries of articulated dendritic wave lobes observed in Mijiaya residue samples

	Sample				
Morphometry	Funnel 1	Pot 2	Pot 3	Pot 4	Pot 5
ND	2	52	24	10	27
NL	33	307	131	97	208
Form factor	0.729788	0.696355	0.668985	0.657271	0.715702
Roundness	0.547273	0.488202	0.455939	0.474625	0.533909
Convexity	0.949152	0.948322	0.947763	0.935229	0.942255
Solidity	0.980485	0.971811	0.971519	0.95774	0.975072
Compactness	0.736576	0.693264	0.669	0.684094	0.726654
Aspect ratio	1.666182	1.948433	2.07529	2.03824	1.737486

ND, the number of articulated dendritics that formed the wave lobes measured; NL, the number of wave lobes measured in each sample.

Table S6. Comparison of mean morphometries of articulated dendritic waves in Mijiaya vessels with the range of mean wave morphometries from selected species from modern comparative species

Reference taxon	Sample	Funnel 1	Pot 2	Pot 3	Pot 4	Pot 5
	ND	2	52	24	10	27
	NL	33	307	131	97	208
Triticum aestivum	Form factor		x	x	x	x
	Roundness	x				x
	Solidity		x	x	x	
	Compactness	x	x			x
	Convexity				x	x
	Aspect ratio					
Triticum dicoccoides	Form factor	x	x	x	x	
	Roundness	x				x
	Solidity				x	
	Compactness	x				x
	Convexity				x	
	Aspect ratio	x				
Triticum dicoccon	Form factor	x	x	x	x	x
	Roundness	x				x
	Solidity		x	x	x	x
	Compactness	x				x
	Convexity		x	x	x	x
	Aspect ratio	x				
Triticum durum	Form factor		x	x	x	
	Roundness					
	Solidity					
	Compactness					
	Convexity				x	
	Aspect ratio					
Triticum monococcum	Form factor	x	x	x		x
	Roundness	x				x
	Solidity	x	x	x	x	x
	Compactness	x				x
	Convexity	x	x	x	x	x
	Aspect ratio	x				
Avena sativa	Form factor		x	x	x	x
	Roundness	x				x
	Solidity		x	x	x	x
	Compactness	x				x
	Convexity				x	x
	Aspect ratio	x				x
Secale cereale	Form factor		x	x	x	
	Roundness	x				x
	Solidity				x	
	Compactness	x				x
	Convexity				x	x
	Aspect ratio	x				
Agropyron cristatum	Form factor	x	x			x
	Roundness	x				x
	Solidity		x	x		x
	Compactness					
	Convexity		x	x		x
	Aspect ratio	x				x
Agropyron mongolicum	Form factor		x			
	Roundness	x				x
	Solidity		x	x	x	
	Compactness	x				x
	Convexity					x
	Aspect ratio	x				x
Elytrigia elongata	Form factor	x				
	Roundness					
	Solidity	x	x	x		x
	Compactness					
	Convexity		x	x		x
	Aspect ratio					

Table S6. Cont.

Reference taxon	Sample	Funnel 1	Pot 2	Pot 3	Pot 4	Pot 5
Leymus secalinus	Form factor	x				x
	Roundness					
	Solidity		x	x		
	Compactness					
	Convexity					x
	Aspect ratio					
Roegneria mayebarana	Form factor	x				x
	Roundness					
	Solidity		x	x		x
	Compactness					
	Convexity	x	x	x		
	Aspect ratio					
Roegneria ciliaris	Form factor	x				
	Roundness					
	Solidity	x				x
	Compactness					
	Convexity					x
	Aspect ratio					
Roegneria pendulina	Form factor	x	x	x	x	x
	Roundness					
	Solidity		x	x		x
	Compactness					
	Convexity					
	Aspect ratio					
	Elongation					
Bromus japonica	Form factor	x	x			x
	Roundness	x				
	Solidity		x	x		
	Compactness	x				
	Convexity					x
	Aspect ratio					
Hordeum vulgare	Form factor	x	x	x	x	x
	Roundness	x	x	x	x	x
	Solidity	x	x	x	x	x
	Compactness	x	x	x	x	x
	Convexity	x	x	x	x	x
	Aspect ratio	x	x	x	x	x
Hordeum bulbosum	Form factor	x				x
	Roundness					
	Solidity	x				
	Compactness					
	Convexity	x	x	x		
	Aspect ratio					
Hordeum comosum	Form factor	x				
	Roundness					
	Solidity		x	x		x
	Compactness					
	Convexity					
	Aspect ratio	x				
Hordeum secalinum	Form factor	x	x			x
	Roundness	x				x
	Solidity	x				
	Compactness	x				x
	Convexity	x	x	x		
	Aspect ratio	x				x
Hordeum distichon	Form factor	x	x	x	x	x
	Roundness	x	x		x	x
	Solidity	x				
	Compactness	x	x		x	x
	Convexity		x	x		
	Aspect ratio	x	x	x	x	x

ND, the number of articulated dendritics that formed the wave lobes measured; NL, the number of wave lobes measured in each sample; x, mean for the sample falls within the range of means for the reference taxon.